Automatic Drift Compensation for Nanoscale Imaging Using Feature Point Matching

Zhuo Diao,[1] Keiichi Ueda,[1,2] Linfeng Hou,[1] Hayato Yamashita,[1] Oscar Custance,[3] and Masayuki Abe[1]
[1)]*Graduate School of Engineering Science, Osaka University, 1-3 Machikaneyama, Toyonaka, Osaka 560-0043, Japan*
[2)]*Tokyo Metropolitan Industrial Technology, Research Institute, 2-4-10 Aomi, Kotoku, Tokyo, 135-0064, Japan*
[3)]*National Institute for Materials Science (NIMS), 1-2-1 Sengen, Tsukuba, Ibaraki 305-0047, Japan*

(Dated: 19 December 2022)

A novel implementation of drift compensation for imaging at the nanoscale is presented. The method is based on computer vision techniques, and hence applicable to any microscope that generates images through a computer interface. The algorithm extracts and matches pairs of feature points from consecutive images to compute and compensate for probe-sample misalignments over time. The protocol also applies selection rules that make it robust against changes in image contrast. We demonstrate our fully-automatic implementation by continuously imaging the same area of a Si(100) surface at the atomic scale with scanning probe microscopy over a period of 25 hours at room temperature, showing that the method is robust even under the presence of non-linear drift or spontaneous changes of the probe apex. We apply our method to study the movement of pairs of tin atoms confined within a half-unit cell of the Si(111)-(7×7) surface and estimate the energy barrier for their diffusion at room temperature.

Advances in nanoscience and nanotechnology are linked to imaging with microscopes at the nanoscale. When exploring nano-structures at room temperature with either scanning transmission electron microscopy, scanning electron microscopy, or scanning probe microscopy, the ever-present thermal drift compromises the time frame for reliable data acquisition. Typical thermal drift in vacuum at room temperature (assuming thermal equilibrium conditions) is, for instance, between 0.3 and 1 Å/min. These values considerably increase for experiments carried out in air or liquid environment. Such thermal drift causes a three-dimensional misalignment between the imaging source and the object under observation, which leads to distorted images[1]. These distortions become critical when exploring specimens of just a few nanometer size[2–4]. To reduce these detrimental effects, one is compelled to either use high-speed data acquisition[5–7] or to implement schemes for the real-time compensation of the thermal drift in three dimensions[8,9]. Similar to thermal drift, piezoelectric creep can also produce image distortions[10,11]. Here, we introduce a novel method for the compensation of probe-sample misalignments that is based on computer vision techniques and therefore universally applicable to any instrument that provides images of objects through a computer interface. Although we demonstrate this method using scanning probe microscopy, it is also possible to apply it to scanning transmission electron microscopy and scanning electron microscopy.

Operation of microscopes in a cryogenic environment —in which sample and probe are cooled down close to the boiling temperature of liquid helium— has been the traditional way to cancel out thermal drift. In such cryogenic conditions landmark feats on scanning probe microscopy (SPM) have been achieved[12–14]. However, on-surface reactions, diffusion of atomic and molecular species and other processes that are in some degree thermally assisted, are more likely to occur well above cryogenic temperatures. To study such process, it is pivotal to compensate the misalignment between the imaging probe and the sample caused by the thermal drift. In SPM, the use of atom tracking to measure the drift and to compensate it by using feedforward techniques[15] has enabled to temporarily keep the relative position of probe and surface with a precision close to the one obtained at cryogenic temperatures so that atom manipulation[3] and reliable spectroscopic measurements[4] were accomplished even at room temperature. The use of feedforward technics requires the thermal drift to be a well-defined function of time so that the probe-surface misalignment can be predicted and compensated over a given time window. For a microscope in thermal equilibrium with the ambient temperature, the thermal drift can be considered almost a linear function of time (i.e., constant drift velocity) over a few minutes, but this linearity is lost over longer periods due to small variations of the ambient temperature. Therefore, the drift velocity must be measured and updated periodically. The method we present here, however, allows imaging the same spot of a sample at the nanometer scale over several days with atomic-level accuracy under the presence of non-linear thermal drift, long-standing piezo creep[16], and even upon changes in the imaging contrast.

The experiments were performed with a home-built SPM operated in ultra-high vacuum and at room temperature. The microscope was controlled by a National Instruments PXIe-7857R unit using a home-built scan and data acquisition software based on LabVIEW and Python. Data and image processing algorithms were implemented using OpenCV[17] and a personal Python library[18]. Atomically clean silicon surfaces were prepared by standard flashing-annealing cycles, and Pt/Ir probes were used to acquire the scanning tunneling microscopy (STM) data presented in this work.

Figure 1 outlines an experiment representative of applying our algorithm. It shows a selection of 9 images extracted from a set of 444 STM topographies that were continuously measured on the same area of the Si(100) surface over a period of

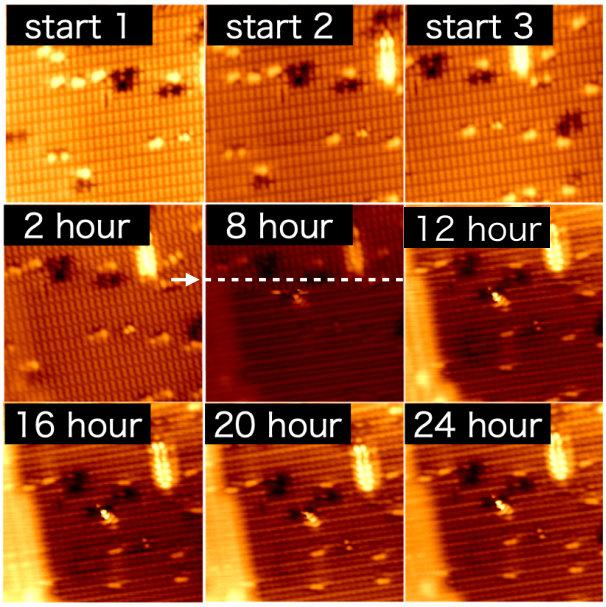

FIG. 1. Selection of STM topographies extracted from a total of 444 images continuously measured over a period of 25 hours tracking the same area of the Si(100) surface using the algorithm presented here (the whole process is presented in a video). The dotted line in the image taken at the 8th hour of the experiment highlights the position at which the image contrast significantly changed due to a spontaneous modification of the probe apex. Image acquisition time, scan area, tunneling current set-point and sample bias were: t=200 s, (11.49 $\times$ 11.49) nm^2, I_t=300 pA and V_s=1.5 V, respectively. The order in which the images were measured and the time since the experiment started are used to label each image.

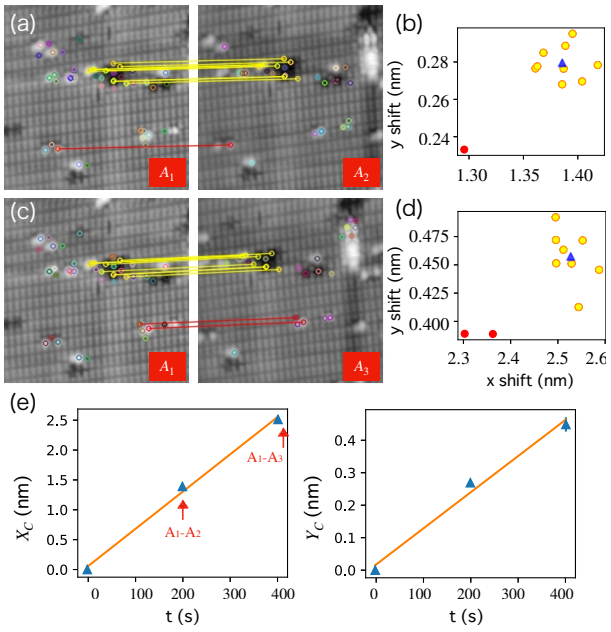

FIG. 2. Illustration of one cycle of our automatic drift correction algorithm. (a) and (c), Acquisition of three consecutive images (A_1,A_2,A_3), extraction of feature points from them (multicolor dots), and matching of pairs of feature points between A_1 and A_2, and A_1 and A_3 (lines connecting dots). (b) and (d), Clustering of the (x, y) coordinates of the relative position between pairs of matched points, and application of a "majority rule" to select a centroid (blue triangle) representative of the relative displacement between images A_1 and A_2, and A_1 and A_3. Yellow lines and points highlight pairs of matched points assigned to the same cluster, and red ones represent matched pairs excluded from the centroid calculation. (e), Estimation of the drift velocity for X and Y scan directions from the X_C and Y_C coordinates of the centroids.

25 hours. The first three images (1, 2, 3) were acquired without drift compensation, as they are used for the first estimation of the drift. In the image taken at the 8th hour of the experiment, the dotted line highlights the position at which a spontaneous modification of the tip apex changed the topographic contrast. Even upon this significant alteration, the algorithm was still able to precisely track the same spot of the surface until the end of the experiment.

Figure 2 illustrates the basic implementation of our fully automated drift correction system. The algorithm comprises two stages: in the first stage, it extracts and matches pairs of feature points from three consecutive images; in the second stage, it groups the matched feature points, calculates the drift velocity, and compensates for the drift. These processes are cyclically repeated every three images. The first three consecutive images are measured without any drift compensation. Once the drift correction is applied, subsequent three-image cycles of the algorithm are carried out with the drift correction on, and the variation of the drift velocity is adjusted with time.

In the first stage of the algorithm, the images are automatically pre-processed by applying a plane fit subtraction followed by a 2D convolution smoothing based on a Gaussian Hann filter with a (11 $\times$ 11) pixel kernel and a σ=1 standard deviation. Feature points from the images (multicolor dots in the STM topographies of Fig. 2) are extracted using the AKAZE detector[19], which offers a precision as good as the KAZE Features detector[20] and a faster calculation speed. Feature points from the first image are matched to the second [Fig. 2(a)] and third images [Fig. 2(c)], respectively. The feature point matching —lines in Figs. 2 (a) and (c)— is done by using OpenCV's Brute-Force matcher with crossCheck enabled: Brute-Force matcher compares the vectors of all feature points of the two images and pairs them by proximity; and crossCheck verifies that the pairing is reciprocal if the image order is exchanged. The relative position between pairs of matched points is calculated and stored on a list of (x, y) coordinates.

In the second stage, the (x, y) coordinates of the relative position between pairs of matched points are grouped by using k-means clustering[21] [see Figs. 2 (b) and (d)]. To define an a priori unknown number (n) of clusters, we use an iterative approach. A two-cluster initialization ($n = 2$) is given to the k-means algorithm. For each of the clusters provided by k-means, we check that the average separation of each of the points of the cluster (g_j) with respect to the cluster's centroid (g_c; the arithmetic mean of all points within the cluster)

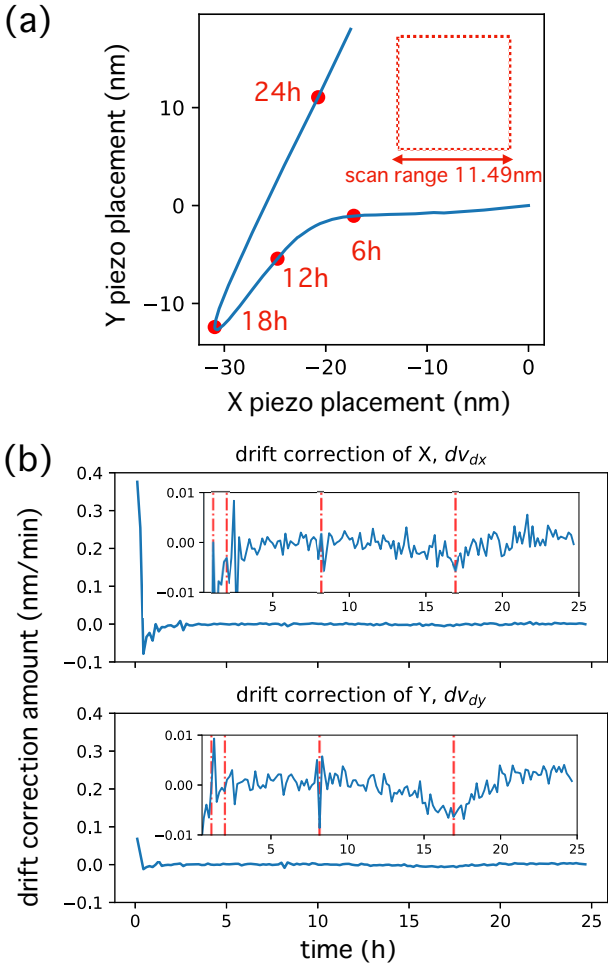

FIG. 3. (a) Trajectory of the drift compensation for the experiment summarized in Fig. 1. Representative time laps are indicated by red spots. The inset denotes the scan area relative to the total trajectory. (b) Drift velocity correction in the X and Y scan directions for the experiment displayed in Fig. 1. The insets represent a zoom-in over the signal excluding the initial stages of the experiment, in which piezo creep dominated the correction. Dotted vertical red lines pinpoint the timing at which the image contrast changed due to spontaneous atomic rearrangements at the probe apex.

is smaller than a given distance d, which is empirically determined according to the image acquisition parameters[22]:

$$d \geq \frac{1}{m} \sum_{1 \leq j \leq m} \sqrt{(g_j - g_c)^2} \qquad (1)$$

with m being the number of points contained within the cluster. If this condition is not fulfilled, n is increased in a unit and fed back into k-means. The iteration on n stops when eq. (1) is satisfied by each of the supplied clusters. Once the number of clusters is defined, a "majority rule" is applied, and the centroid of the cluster containing the largest number of points is chosen to characterize the relative displacement of images A_2 and A_3 with respect to A_1. In case the number of pairs of matched featured points is lower than five, the algorithm selects all the matched points to calculate the centroid. The slope of a linear regression[9] fitting of the X_C and Y_C coordinates of the centroids with respect to the corresponding image timestamp (t) [Fig. 2(e)] supplies the drift velocity in the X and Y scan directions, respectively. The drift is then compensated by applying a linear feedforward signal into the X and Y channels, and the acquisition of three new images to start the next loop of the algorithm is performed. Each of these loops produces a correction to the drift velocity, dv_{dx} and dv_{dy}, that is supplied to the feedforward protocol to lock on the same surface area for long periods of time.

Figure 3 displays the drift compensation report for the experiment summarized in Fig. 1. The trace depicted in Fig. 3(a) reveals a strong non-linear behavior of the drift over the 25 hours the algorithm was tracking the same surface spot. This non-linearity over long periods does not represent a challenge to our method, because the drift correction is updated every three images. The graphs in Fig. 3(b) show the correction to the drift velocity in the X and Y scan directions during the 25 hours experiment. At the initial stages of the tracking, both components display a spike, which is more prominent over the X scan direction. These rapid changes in the drift velocity are due to piezo creep originated from moving the scanner to the desired surface area before starting the algorithm. After six loops (i.e, approximately one hour) the creep effect became negligible, and the drift velocity stabilized with a standard deviation of 3.11 pm/min in the X direction and 2.79 pm/min in the Y direction, respectively, see insets in Fig. 3(b). These values demonstrate that our method has enough precision and stability to perform sub-angstrom order drift compensation.

It is possible to pause the imaging loop to carry out a variety of experiments, such as point spectroscopy[4], bias pulse manipulations[23] and, depending on the drift condition, even three-dimensional spectroscopic measurements[24]. In this case, the last drift velocity calculated will be used to compensate for the drift until the imaging loop is restored[25].

Unlike other approaches to compensate for the drift, such as using cross-correlation between images[26], our method is quite robust against changes in image contrast and resolution. This characteristic is demonstrated in Fig. 4, where the feature point matching from the three-image loops before (A_{139},A_{140},A_{141}) and during (A_{142},A_{143},A_{144}) the spontaneous probe modification displayed in Fig. 1 is presented. The atomic reconfiguration occurring at the probe apex during the acquisition of image A_{142} led to a change in the atomic contrasts and to a different set of pairs of featured points, see Figs. 4(e) and (g). Even upon this dramatic probe change, the algorithm was able to cluster the newly detected pairs of points, apply the "majority rule" [points and lines in yellow in Fig. 4 (e) and (g)] and update the drift velocity. In the insets of Fig. 3(b), the dotted vertical red lines indicate the occurrence of spontaneous probe modifications similar to the one described in Fig. 4. So far, we have not found any situation in which a probe change was catastrophic enough for the algorithm to fail: there are always enough pairs of feature points produced to ensure the correct execution of the algorithm. However, as a safety measurement, in case no feature

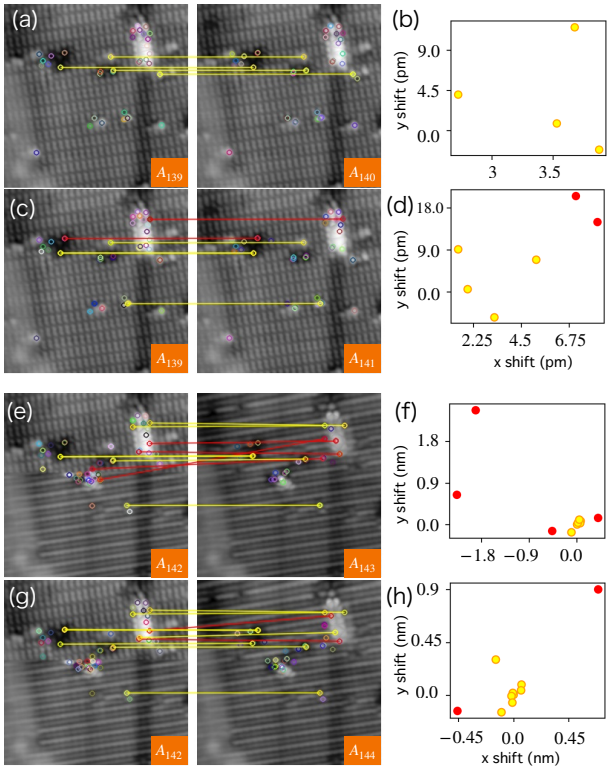

FIG. 4. Feature point matching and clustering of pairs of matched points before (a) to (d) and during (e) to (h) the probe-induced image contrast change displayed in Fig.1.

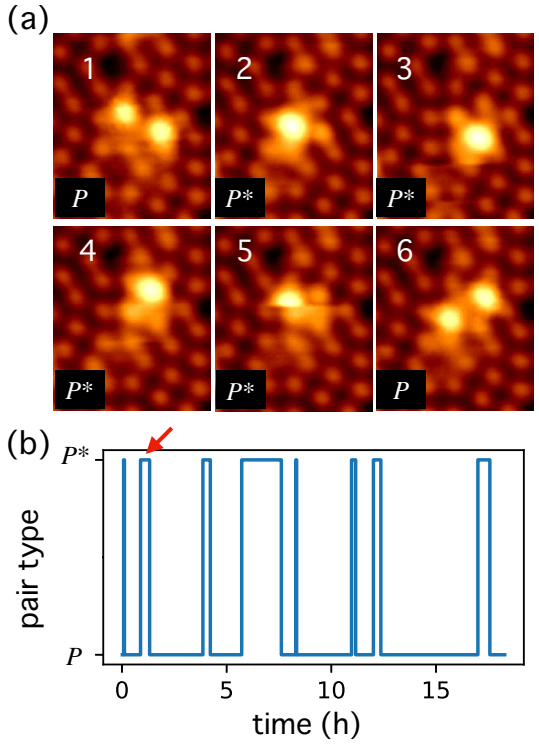

FIG. 5. (a) Series of consecutive images demonstrating the reversible switching of a pair of Sn atoms between two types of adsorption configurations, P (1 and 6) and P^* (2 to 5), on a faulted half-unit cell of the Si(111)-(7×7) surface. Images 2 to 5 show the diffusion of the pair of Sn atoms in a P^* configuration between three equivalent adsorption positions within the half-unit cell. (g) Telegraphic switching behavior of the pair of Sn atoms displayed in (a) between the P and P^* configurations characterized over a period of 18 hours. The red arrow points to the event at which the series of images in (a) was acquired. Image acquisition time, tunneling current set-point and sample bias were t=66 s, I_t=200 pA and V_s=1.5 V, respectively. The image size is (2.43 × 3.80) nm^2.

points are matched, the algorithm will not compensate for the drift and it will restart the acquisition of three new images to recalculate the drift velocity.

We applied our drift compensation algorithm to study the switching of pairs of Sn atoms between two adsorption configurations on the Si(111)-(7×7) surface[27]. The samples were prepared following the procedure described in Ref. 27[27]. We explored this surface system in several experimental sessions, in each of them imaging an area of interest at the surface for long periods of time. We have been able to track the same surface spot as long as for three consecutive days. Figure 5 summarizes one of these measurement sessions, in which we performed an 18-hour observation of the same surface area, generating a total of 927 images, with an acquisition time of 66 sec per frame plus an idle time of 5 sec between images to reduce piezo creep[10]. During this 18-hour experiment, we characterized the switching behavior of a pair of Sn atoms trapped within a half-unit cell of the Si(111)-(7×7) surface. This pair of Sn atoms was seen in two adsorption configurations: P and P^* [Fig. 5(a)]. We identified reversible transitions between P and P^* configurations that occur at a relatively low frequency, as it is shown in the six panels of Fig. 5(a). We also detected jumps of the pair in a P^* configuration between three equivalent adsorption sites with an occurrence close to our fastest image speed, see images 2 to 5 in Fig. 5(a). Therefore, we focused our analysis on the reversible transitions $P \leftrightarrow P^*$, because at the image speed we conducted the experiment jumps of the pair in a P^* configuration can be missed during imaging. In Fig. 5(b), we have quantified the transitions $P \rightarrow P^*$ and $P^* \rightarrow P$ during the 18 hours we were imaging the same surface area. Our results suggest that the Sn atoms prefer to stay in a P configuration longer than in a P^* one, thus the P configuration seems to be more stable than the P^* one.

We have made a rough estimation of the energy barrier for both transitions assuming that they are thermally activated and follow an Arrhenius equation ($\Gamma = \Gamma_0 \exp[-E_g/kT]$), with Γ_0 being the attempt frequency, E_g the energy barrier for the transition, k the Boltzmann constant and T the absolute temperature. In the absence of a variable temperature STM that would allow us to measure the switching rate at several temperatures to estimate both the attempt frequency and the energy barrier, we have adopted values for Γ_0 from the literature to make a rough estimation of the energy barrier. In the case of the rotation of pairs of Pb atoms within a half-

unit cell of the Si(111)-(7×7) surface, an attempt frequency of 10^{12} jumps/pair/second was experimentally obtained[28]. Considering this value of Γ_0 and that the experiments were done at room temperature (293 K), we obtain an energy barrier of 0.91±0.01 eV for the $P \rightarrow P^*$ transition and a value of 0.86±0.03 eV for the $P^* \rightarrow P$ one. The error in these values is provided by the statistical standard deviation of the time spent by the Sn pair in a given configuration. This experiment is a showcase for the potential of our drift compensation algorithm to obtain the physical properties of surface systems.

We have put forward a new algorithm for the real-time automatic compensation of drift at the atomic scale using feature point detection in images. Because we deploy matching and clustering of feature points between three consecutive images, our approach is robust against contrast changes by slight modifications of both probe and surface. At variance with previously reported approaches[15], our method can track the same surface area for days with sub-angstrom precision even under a no-linear drift behavior just by imaging. Additionally, since our method is based on computer vision technics, its application is not limited to scanning probe microscopy, but it can also be implemented in other microscopy setups such as scanning electron microscopy or transmission electron microscopy. Our algorithm is open source and available elsewhere[29].

This work was supported in part by a Grant-in-Aid for Scientific Research (19H05789, 21H01812, 21K18876) from the Ministry of Education, Culture, Sports, Science and Technology of Japan (MEXT) and by NIMS grants (PF2010, PF3130 and QN3510). A part of this work was also supported by JST SPRING (JPMJSP2138).

[1] C. T. Herbschleb et al., Review of Scientific Instruments **85**, 083703 (2014).
[2] E. Hill, B. Freelon, and E. Ganz, Phys. Rev. B **60**, 15896 (1999).
[3] Y. Sugimoto et al., Science **322**, 413 (2008).
[4] Y. Sugimoto et al., Nature **446**, 64 (2007).
[5] L. M. Picco et al., Nanotechnology **18**, 044030 (2006).
[6] L. Gura et al., Applied Physics Letters **119**, 251601 (2021).
[7] L. Gura et al., Phys. Rev. B **105**, 035411 (2022).
[8] M. Abe, Y. Sugimoto, O. Custance, and S. Morita, Nanotechnology **16**, 3029 (2005).
[9] P. Rahe et al., Review of Scientific Instruments **82**, 063704 (2011).
[10] M. S. Rana, H. R. Pota, and I. R. Petersen, IEEE/ASME Transactions on Mechatronics **20**, 1458 (2015).
[11] S. B. Park, S. S. Park, and G. P. Carman, Linear and nonlinear behavior of piezoelectric materials, in *Proc.SPIE*, volume 2715, 1996.
[12] D. M. Eigler and E. K. Schweizer, Nature **344**, 524 (1990).
[13] M. A. Lantz et al., Phys. Rev. Lett. **84**, 2642 (2000).
[14] L. Gross, F. Mohn, N. Moll, P. Liljeroth, and G. Meyer, Science **325**, 1110 (2009).
[15] M. Abe, Y. Sugimoto, O. Custance, and S. Morita, Appl. Phys. Lett. **87**, 173503 (2005).
[16] D. Croft, G. Shed, and S. Devasia, Journal of Dynamic Systems, Measurement, and Control **123**, 35 (1999).
[17] G. Bradski, Dr. Dobb's Journal of Software Tools (2000).
[18] Spmutil, see `https://github.com/DIAOZHUO/SPMUtil` for installation and basic usage.
[19] P. F. Alcantarilla, J. Nuevo, and A. Bartoli, Fast explicit diffusion for accelerated features in nonlinear scale spaces, in *British Machine Vision Conference, BMVC 2013, Bristol, UK, September 9-13, 2013*, edited by T. Burghardt, D. Damen, W. W. Mayol-Cuevas, and M. Mirmehdi, BMVA Press, 2013.
[20] P. F. Alcantarilla, A. Bartoli, and A. J. Davison, Kaze features, in *Proceedings of the 12th European Conference on Computer Vision - Volume Part VI*, ECCV'12, pages 214–227, Berlin, Heidelberg, 2012, Springer-Verlag.
[21] D. Arthur and S. Vassilvitskii, K-means++: The advantages of careful seeding, in *Proceedings of the Eighteenth Annual ACM-SIAM Symposium on Discrete Algorithms*, SODA '07, pages 1027–1035, USA, 2007, Society for Industrial and Applied Mathematics.
[22] The value of the distance d is empirically tuned depending on the size and resolution of the images. In this work, we used a value d=1nm for (256 × 256) pixel images of (20 × 20) nm^2 scan area.
[23] N. Pavlicek et al., Nature Nanotech. **12**, 308 (2017).
[24] B. J. Albers et al., Nature Nanotech. **4**, 307 (2009).
[25] Our algorithm is not rotation or scale-invariant: if the image orientation or its scale is changed dur- ing the experiment, the feature point matching will not provide a reliable result upon restoring the imaging loop.
[26] I. Horcas et al., Review of Scientific Instruments **78**, 013705 (2007).
[27] O. Custance, I. Brihuega, J. Gómez-Rodríguez, and A. Baró, Surface Science **482-485**, 1406 (2001).
[28] O. Custance et al., Phys. Rev. B **67**, 235410 (2003).
[29] The source code and an example are available at `https://github.com/DIAOZHUO/drift_compensation_by_feature_point_matching`.